Earthquakes and Structures, *Vol. 16, No. 5 (2019) 563-573*
DOI: https://doi.org/10.12989/eas.2019.16.5.563

Simulation method of ground motion matching for multiple targets and effects of fitting parameter variation on the distribution of PGD

Shaoqing Wang, Ruifang Yu*, Xiaojun Li and Hongshan Lv

Institute of Geophysics, China Earthquake Administration, No. 5, Minzu Daxue South Road, Haidian District, Beijing, 100081, China

(Received October 4, 2018, Revised March 26, 2019, Accepted March 28, 2019)

Abstract. When generating spectrum-compatible artificial ground motion in engineering practices, the effect of the variation in fitting parameters on the distribution of the peak ground displacement (PGD) has not yet drawn enough attention. In this study, a method for simulating ground motion matching for multiple targets is developed. In this method, a frequency-dependent amplitude envelope function with statistical parameters is introduced to simulate the nonstationarity of the frequency in earthquake ground motion. Then, several groups of time-history acceleration with different temporal and spectral nonstationarities were generated to analyze the effect of nonstationary parameter variations on the distribution of PGD. The following conclusions are drawn from the results: (1) In the simulation of spectrum-compatible artificial ground motion, if the acceleration time-history is generated with random initial phases, the corresponding PGD distribution is quite discrete and an uncertain number of PGD values lower than the limit value are observed. Nevertheless, the mean values of PGD always meet the requirement in every group. (2) If the nonstationary frequencies of the ground motion are taken into account when fitting the target spectrum, the corresponding PGD values will increase. A correlation analysis shows that the change in the mean and the dispersion values, from before the frequencies are controlled to after, correlates with the modal parameters of the predominant frequencies. (3) Extending the maximum period of the target spectrum will increase the corresponding PGD value and, simultaneously, decrease the PGD dispersion. Finally, in order to control the PGD effectively, the ground motion simulation method suggested in this study was revised to target a specified PGD. This novel method can generate ground motion that satisfies not only the required precision of the target spectrum, peak ground acceleration (PGA), and nonstationarity characteristics of the ground motion but also meets the required limit of the PGD, improving engineering practices.

Keywords: simulation of ground motion; peak ground displacement; nonstationary; spectrum compatible; multiple targets

1. Introduction

The inputs for seismic design are usually derived from two sources: strong earthquake records and simulated ground motion. Due to sparse data with uneven spatial and temporal distributions, real records cannot satisfy the various requirements of seismic design, resulting in the urgent demand for artificial strong ground motion data. Based on engineering practices, methods for synthesizing spectrum-compatible artificial ground motion were developed rapidly (Preumont 1984, Naeim and Lew 1995, Carballo and Cornell 2000, Zhao *et al*. 2006, Hancock *et al*. 2006, Gao *et al*. 2014). In addition to the often-used trigonometric method in which the target spectra are modified using a frequency domain method, many other new methods were proposed. For example, Ghaboussi and Lin (1998) proposed a method that generates spectrum-compatible ground motions using neural networks. Mukherjee and Gupta (2002) proposed a wavelet-based procedure in which a recorded accelerogram can be decomposed into the desired number of time histories with nonoverlapping frequencies, and then each of the time histories can be scaled to match the response spectrum of the revised accelerogram with a specified design spectrum. Cacciola (2010) proposed a method that generates fully nonstationary earthquakes by adjusting fully nonstationary counterparts, modeled using earthquake records with a random corrective process, which can make the time-history spectrum compatible. In addition, baseline correction should be carried out as a part of the simulation procedure (Converse and Brady 1992, Iwan *et al*. 1985, Boore 2005). However, the corresponding peak ground displacement (PGD) of the simulated ground motion has drawn less attention in the aforementioned spectrum-matching methods. In engineering practices, in addition to peak ground acceleration (PGA) and peak ground velocity (PGV), PGD also has a distinct influence on the nonlinear response of some long-period structures, such as bridges, buried pipelines, storage tanks and isolated structures (Pineda-Porras and Ordaz 2007, Tondini and Stojadinovic 2012, Han *et al*. 2013, Guan *et al*. 2015). For example, Hall *et al*. (1995) simulated an Mw7.0 earthquake and found that large, rapid displacement pulses of near-source ground motion will increase the collapse potential of flexible buildings. Milana *et al*. (2008) studied the long-period ground motion of volcanic earthquakes at Mt. Etna, Italy, and found that large ground displacements caused selective

*Corresponding author, Professor
E-mail: yrfang126@126.com

ISSN: 2092-7614 (Print), 2092-7622 (Online)

damage to medium-sized reinforced concrete buildings and elements, such as church façades. Buratti and Tavano (2014) studied the dynamic buckling and seismic fragility of anchored steel tanks and found that PGD is currently the most efficient and accurate measurement of intensity to determine the maximum relative displacement of the tank wall. Therefore, in seismic design, one should also consider the effects of PGD on the response of structures with long natural periods. For example, the Chinese Code for Seismic Design of Urban Rail Transit Structures (Code, GB 50909-2014) sets horizontal ground motion PGD limits for various site conditions for the longer natural periods of rail transit structures.

In practical engineering applications, by only fitting the response spectrum as the target in time-history acceleration simulations, we do not know whether the corresponding PGD can meet the requirements. Therefore, this study mainly focuses on the following aspects. First, we develop a method for generating artificial ground motion with required spectral nonstationary characteristics. Second, we optimize the reasonable sample size of simulated ground motion. Third, we analyze the effects of the different nonstationary simulated ground motion parameter settings and the variation of the target spectrum's maximum period on the distribution of PGD. Finally, we propose a method to control the PGD directly in the simulation. This novel fitting method can generate ground motion that satisfies not only the required precision of the target spectrum, PGA, and nonstationarity characteristics of the ground motion but also the required limit of the PGD, improving engineering practices.

2. Method for simulating earthquake ground motion based on the frequency-dependent amplitude envelope function

2.1 Basic formula for simulating nonstationary earthquake ground motion

To reflect the time-varying nature of ground motion frequencies, the following stochastic process model is adopted (Nigam and Mark 1984)

$$y(t)=\int_{-\infty}^{+\infty}B(t,\omega)\mathrm{e}^{i\omega t}\mathrm{d}F(\omega) \tag{1}$$

where $i=\sqrt{-1}$, $B(t,\omega)$ is a deterministic time-frequency modulating function, representing the absolute amplitude of the seismic time series, and $\mathrm{d}F(\omega)$ denotes a zero-mean and mutually independent orthogonal increment process with

$$E[dF(\omega)]=0 \tag{2}$$

$$E[dF^{*}(\omega_1)dF(\omega_2)]=\delta(\omega_1-\omega_2)S(\omega_1)d\omega_1 d\omega_2 \tag{3}$$

where $E[.]$ is the ensemble average, $\delta(.)$ is the Dirac delta function, * is the complex conjugate, and $S(\omega)$ is the power spectral density function of $\mathrm{d}F(\omega)$.

In engineering practices, these expressions are logical only when the time-frequency modulation function is real and nonnegative, i.e.

$$B(t,\omega)\in R, B(t,\omega)\geq 0 \tag{4}$$

Assume that for a given ω_k, $B(t,\omega_k)$ is normalized as

$$\max[B(t,\omega_k)]=1 \tag{5}$$

$B(t,\omega_k)$ determines only the shape of the envelope at ω_k, while the amplitude for ω_k is determined by $S(\omega)$. Therefore, the artificial ground motion can be generated using Eq. (1) and adopting the following trigonometric equation

$$y(t)=\sum_{k=1}^{n}2B(t,\omega_k)\sqrt{S(\omega_k)\Delta\omega}\cos(\omega_k t+\phi_k) \tag{6}$$

in which ω_k is the discrete circular frequency, $\Delta\omega$ is the frequency increment, and ϕ_k is the random phase with uniform distribution from 0 to2π. If $B(t,\omega_k)$ is replaced by the often-used intensity envelope function, which is only time-dependent (Amin and Ang 1968, Iyengar and Iyengar 1968, Rezaeian and Kiureghian 2008, Rezaeian and Kiureghian 2010), then Eq. (6) can represent only the temporal nonstationarity of the ground motion, that is

$$y(t)=E(t)\sum_{k=1}^{n}2\sqrt{S(\omega_k)\Delta\omega}\cos(\omega_k t+\varphi_k) \tag{7}$$

where $E(t)$ is the intensity amplitude envelope.

Clearly, if the time-frequency joint distribution of $B(t,\omega)$ at different ω_k can be estimated reasonably, based on engineering applications, it is not difficult to solve Eq. (6).

2.2 Frequency-dependent amplitude envelope function $B(t,\omega)$ with statistical parameters

The instantaneous spectrum, which can be used to describe both the temporal and spectral nonstationary characteristics, has been developed (Boashash 1992a, b, Newland 1994, Huang *et al*. 1998, Castagna *et al*. 2003). However, due to the complexity of describing the time-frequency joint distribution function of ground motion, it is difficult to extract statistically significant parameters, limiting its application in engineering practices. Therefore, the predominant frequency, $F_p(t)$, was proposed to simulate the approximate time-varying frequencies of ground motion (Yu *et al*. 2015). $F_p(t)$ represents the frequencies corresponding to the maximum amplitudes on the time-frequency joint spectrum in a sampled time series $(t_1, t_2, \cdots, \text{and } t_n)$. Based on the analysis of the recorded data, a model of the time-dependent predominant frequency was proposed as

$$F_p(t)=f_0+p\mathrm{e}^{-st}\sin(\omega t) \tag{8}$$

where f_0, p, s, and ω together determine the shape of the time-varying curve of the predominant frequencies and can be chosen from a list of 90 groups of statistical regression results, which were obtained by analyzing 10545 recorded motions in the Next Generation Attenuation (NGA) project global database of accelerograms, based on various magnitudes, distances, site conditions and directions (Yu *et al.* 2015). As an example, the variations in $F_p(t)$ for

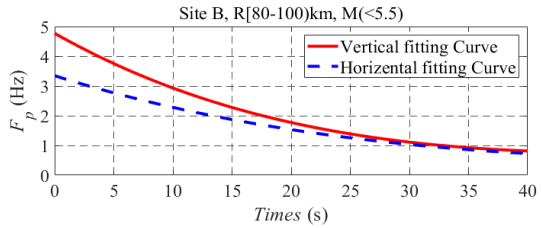

Fig. 1 Variation and fitting of predominant frequency

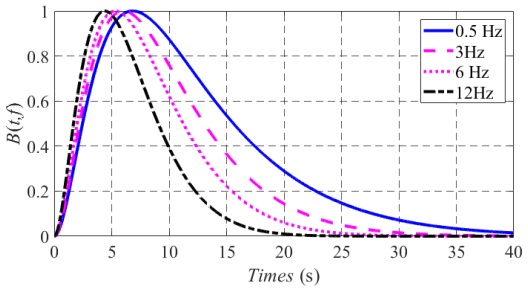

Fig. 2 Variation of frequency-dependent amplitude envelope function at different frequency

M=[6.5, 7.0) and R=(60-80) km for Site B are plotted in Fig. 1, in which the values of $F_p(t)$ in the horizontal and velocity directions are represented respectively.

For a given time-series, t_k, the frequency-dependent spectrum can be described by a single-peak function as

$$L(t_k, f) = \frac{f}{F_p(t_k)} \mathrm{e}^{-\frac{f - F_p(t_k)}{F_p(t_k)}} \tag{9}$$

where f is the frequency and $F_p(t_k)$ is the predominant frequency at the sampling time, t_k, calculated by Eq. (8).

If the amplitude variation in the seismic ground motion is described by $E(t)$, the time-frequency joint distribution of the earthquake ground motion can be defined as

$$WB(t, f) = E^2(t) L(t, f) \tag{10}$$

in which the model shape and parameters can be chosen according to the engineering requirements. Then, the frequency-dependent envelope function of ground motion, $B(t, f_k)$, corresponding to f_k can be obtained by normalizing $WB(t, f_k)$, that is

$$B(t, f_k) = \frac{WB(t, f_k)}{\max[WB(t, f_k)]}, k = 1,2,3,\cdots \tag{11}$$

The variations of $B(t, f)$ at 0.5, 3, 6 and 12 Hz are shown in Fig. 2. It can be seen that the frequency-dependent amplitude envelope functions emphasize the effects of the low-frequency components of ground motion, especially in the later seismic actions.

2.3 Adjustment of nonstationary ground motion based on multiple targets

Initial acceleration time-history, generated by Eq. (6) or Eq. (7), should be adjusted to not only reflect the time-frequency characteristics of the actual earthquake but also meet the fitting precision for multiple targets, such as the response spectrum, PGA, etc. Compared with methods that adjust in the frequency domain, slight adjustment in the time domain does not influence the time when the peak response occurs. Additionally, time-domain methods can retain the original nonstationarity and duration of the initial ground motion and simultaneously make it spectrum compatible. Therefore, we adopted a time-domain method to adjust the initial synthesized ground motion with the aforementioned frequency-dependent amplitude envelope function $B(t, \omega)$.

Supposing that the acceleration time-history after i adjustments is $a_g^i(t)$, the difference between the modified and target spectra at ω_k is expressed as $\delta S_a(\omega_k)$. Then $\delta S_a(\omega_k)$ can be computed through the Duhamel's integral (Lilhanand and Tseng 1988)

$$\delta S_a(\omega_k) = \int_0^{t_m} \delta a_g^i(t) h(t_m - t) \mathrm{d}t \tag{12}$$

where t_m is the time corresponding to the peak acceleration of the structural response. $\delta a_g^i(t)$ is the incremental acceleration history and can be defined as r times of an unit adjusting time-history, that is

$$\delta a_g^i(t) = r \cdot h(t_m - t) B(t, \omega_k), t \le t_m \tag{13}$$

where r is an unknown constant coefficient to be determined, $B(t, \omega_k)$ is used to retain the time-varying frequency characteristics of ground motion, and $h(t_m - t)$ is the well-known damped unit-impulse response function as it expresses the response of damped single degree of freedom system (Clough and Penzien 1975), which can be obtained by

$$h(t_m - t) = \mathrm{e}^{\zeta \omega_k (t - t_m)} \cos[\omega_{Dk}(t_m - t) + \phi_k] \tag{14}$$

where ζ is the damping ratio, ϕ_k is the initial phase of the accelerate impulse and $\omega_{Dk} = \omega_k \sqrt{1 - \zeta^2}$ is the free-vibration frequency of the damped system.

From Eqs. (12) - (13), $\delta S_a(\omega_k)$ becomes

$$\delta S_a(\omega_k) = Cr \tag{15}$$

where C is the response of the unit adjusting time-history

$$C = \int_0^{t_m} h^2(t_m - t) B(t, \omega_k) \mathrm{d}t \tag{16}$$

Having computed C, Eq. (15) can be solved for r.

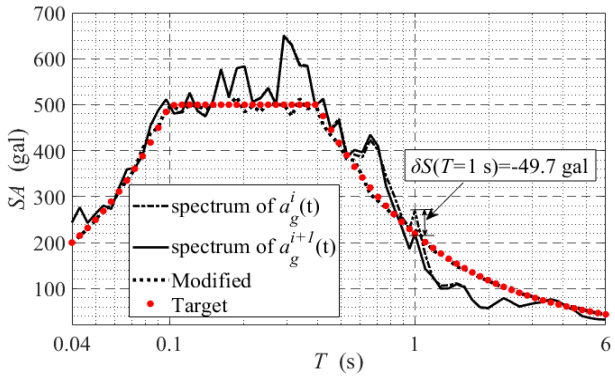

Fig. 3 Response spectra modified by unit impulse-response functions

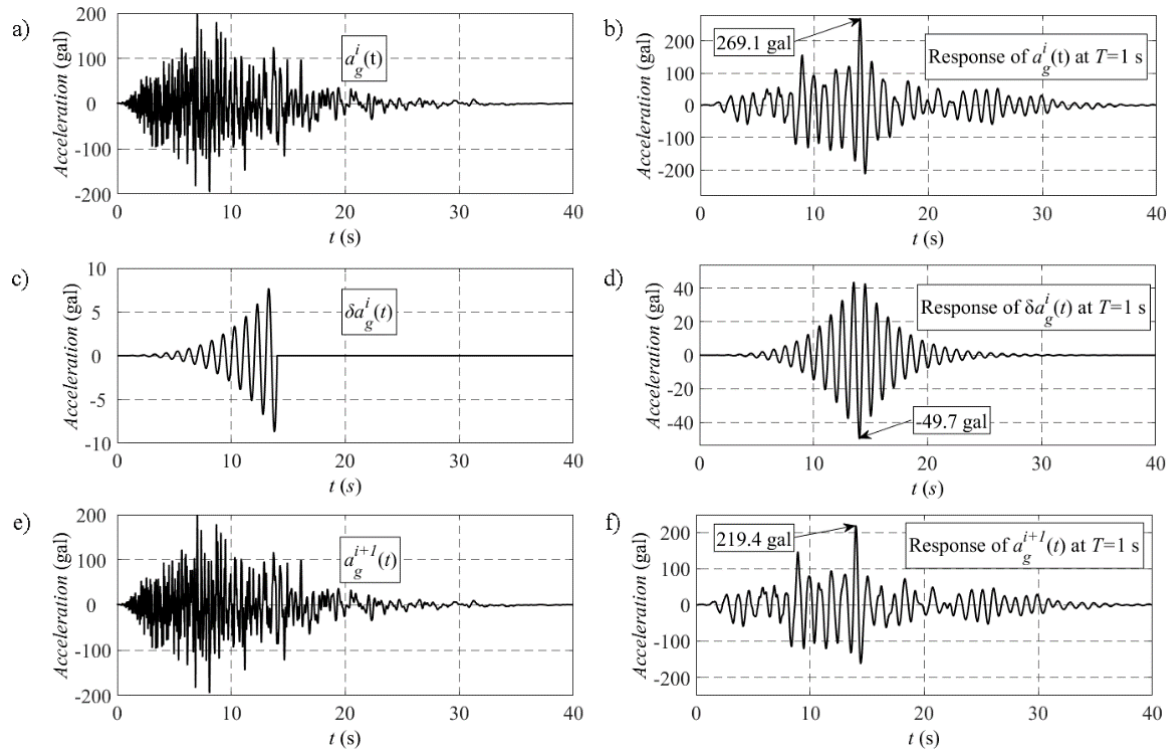

Fig. 4 Procedure of adjustment, (a) Acceleration time-history $a_g^i(t)$ before adjustment. (b) Structural acceleration response time-history before adjustment. (c) The incremental acceleration time-history $\delta a_g^i(t)$. (d) The response time-history of the incremental acceleration time-history $\delta a_g^i(t)$. (e) Acceleration time-history after adjustment which is the superposition of $a_g^i(t)$ and $\delta a_g^i(t)$. (f) Acceleration response time-history under the earthquake input $a_g^{i+1}(t)$

Thus, we can get $\delta a_g^i(t)$ from Eq. (13).

In the method discussed above, if we replace the frequency-dependent amplitude envelope function, $B(t,\omega_k)$, with the often-used intensity envelope function, $E(t)$, then Eq. (13) will degenerate into a formula that can only represent the temporal nonstationarity, that is

$$\delta a_g^i(t) = r \cdot h(t_m - t)E(t), t \le t_m \tag{17}$$

Then, we can obtain the adjusted time history by using

$$a_g^{i+1}(t) = a_g^i(t) + \delta a_g^i(t) \tag{18}$$

This adjustment process can be illustrated by the following example. For a target spectrum as shown in Fig. 3, after i-th adjustments, the acceleration time history $a_g^i(t)$ is plotted in Fig. 4(a). For a given control period $T = 1$s, the fitting for the target response spectrum will be achieved through the following adjustments:

(1) Calculate the response time-history of single-degree-of-freedom system under earthquake input $a_g^i(t)$, reaching the peak value 269.1 gal at $t_\mathrm{m} = 14$ s, as shown in Fig. 4(b).

(2) Determine the difference between the peak response and the target at $= 1$ s , that is, $\delta S_a(\omega_k) = -49.7$ gal, as shown in Fig. 3.

(3) According to Eq. (13), the incremental acceleration time-history $\delta a_g^i(t)$, as shown in Fig. 4(c), can be obtained, in which $C = -4.62$ gal, $r = 10.77$. Thus, the required precision of the calculated spectrum can be satisfied at $T = 1$ s, The response time-history under earthquake input $\delta a_g^i(t)$ is plotted in Fig.4 (d). It can be seen that the peak response, -49.7 gal, occurs at 14 s.

(4) The new acceleration time-history,$a_g^{i+1}(t)$, can be obtained by Eq. (18), as shown in Fig. 4(e).

(5) Calculate the response time-history of single-degree-of-freedom system under earthquake input $a_g^{i+1}(t)$, as shown in Fig.4(f), the peak value of response equaling to the target at $t_m = 14$ s.

The response spectrum after the adjustment is plotted as the short-dash line in Fig. 3. Then, $a_g^{i+1}(t)$ is taken as the new earthquake input and used to calculate and adjust the next controlling period in Eqs. (13) - (18). It should be noted that the incremental acceleration time-history should adjust the initial ground motion as little as possible to retain the characteristics of initial ground motion. Therefore, the incremental acceleration time-history defined in this method only retain the part before the peak occurs, as shown in Fig.4 (c).

Moreover, because the time-varying frequency is controlled in both the initial motion synthesis and the adjustment processes, the final spectrum-compatible ground motion can represent the time-varying predominant frequency required, as shown in Fig. 5.

In the adjustment procedure, every adjustment step will influence the response of other controlling periods. Thus, we have to repeat the aforementioned processes to relieve this influence until the precision between the modified and target spectra meets the requirement (the solid line in Fig. 3).

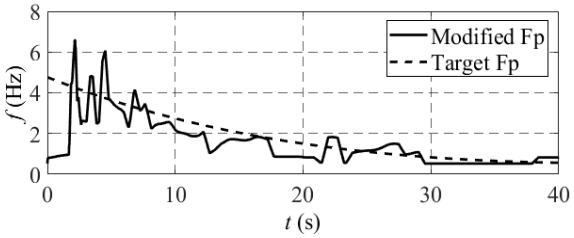

Fig. 5 Comparison of time-varying predominant frequency $F_p(t)$ between modified and target F_p

3. Discussion of the sample size of simulated ground motion

According Eq. (6) and Eqs. (12)-(18), we can obtain acceleration time-history $a(t)$ satisfying multiple targets, such as response spectrum, PGA, and the time-varying frequency characteristics, etc. Based on acceleration time-history $a(t)$, we can obtain the corresponding velocity time-history $v(t)$ and displacement time-history $u(t)$ by acceleration integration. Except for PGA, peak velocity and displacement of ground motion, that is, PGV and PGD, defined as the maximum absolute values of $v(t)$ and $u(t)$, are the most commonly applied intensity measure parameters of ground motion in earthquake engineering, especially, for long-period structures. However, when generating spectrum-compatible artificial ground motion, the PGD is generally not controlled. As random phases and different methods are adopted in the simulation of acceleration time-history, the corresponding PGD will vary distinctively. This makes us have to study the changes of PGD with fitting parameters of ground motion. In order to make the statistical results credible, the sample size of simulated ground motion should be studied to find out how many PGD samples can represent the actual distribution.

In this section, the target spectrum used to simulate the ground motions is defined as

$$S_a(T) = A_{\max}\beta(T) \tag{19}$$

where $A_{\max}$ is the PGA and $\beta(T)$ is an amplification factor, as shown in Fig. 6 in which T is the period, T_g is the characteristic period of the acceleration response spectrum, and γ is the attenuation coefficient. In this study, $A_{\max} = 200$ gal, $T_1 = 0.1$ s, $T_g = 0.4$ s , $T_m = 6$ s, $\gamma = 1.0$, and $\beta_m = 2.5$.

First, 90 acceleration time-histories were generated using Eqs. (6), (13) and (18) to satisfy the target spectrum. The fitting conditions are as follows:

1) The initial ground motions were generated by adopting random phases, and baseline correction was carried out in the simulation.

2) Only the temporal nonstationary characteristics of ground motion were controlled. The intensity envelope function we chose adopted a three-stage form, as shown in Fig. 7, with $t_1 = 3.5$ s, $t_2 = 17.5$ s and $t_d = 40$ s.

3) For the sake of the availability of the samples, we ensured that every acceleration time-history was not correlated with each other.

4) Errors between the target and modified spectra were constrained to less than 5 percent.

5) The PGD was not controlled in the simulation of ground motion.

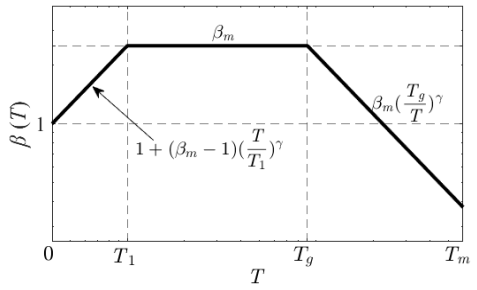

Fig. 6 Amplification factor

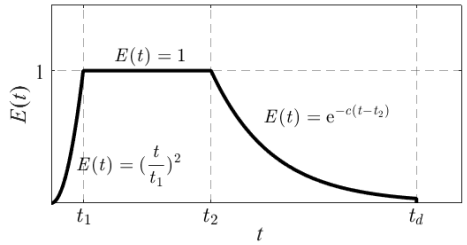

Fig. 7 Intensity envelope function

Table 1 Basic statistical values of PGDs with small sample-sizes

	Group ID	*Number*	*μ (cm)*	*Min (cm)*	*σ (cm)*
	1	*7*	*19.9*	*15.8*	*3.9*
Sampling A	*2*	*15*	*18.9*	*14.7*	*3.4*
	3	*30*	*18.4*	*12.2*	*3.6*
	4	*7*	*16.8*	*12.2*	*4.3*
Sampling B	*5*	*15*	*18.2*	*12.2*	*4.1*
	6	*30*	*17.5*	*11.9*	*3.8*

Then, the corresponding velocity and displacement time-histories can be obtained by integrating 90 accelerations satisfying the target response spectrum and PGA. So, 90 PGDs, defined as the maximum absolute values of the displacement time histories, were obtained for discussion on the reasonable sample size. Based on site conditions and PGA, the limit of minimum PGD value in this case is 13 cm, in accordance with Code GB50909-2014.

We first studied a small sample size situation. The artificial time-histories were randomly sampled twice into six groups. As shown in Table 1, Samples A and B represent two different samplings, and the numbers of time-histories are 7, 15, and 30 for different groups, respectively. Then, we statistically analyzed the PGD values corresponding to the acceleration time-histories in each group. The results are listed in Table 1 in which μ is the mean value, Min is the minimum value, and σ is the standard deviation. The variations of these parameters are plotted in Fig. 8. It can be seen that the mean values of all six groups are higher than the limit value, 13 cm, but PGDs lower than the limit value exist. That is, the risk of an existing PGD lower than the limit value cannot be neglected. Therefore, in engineering

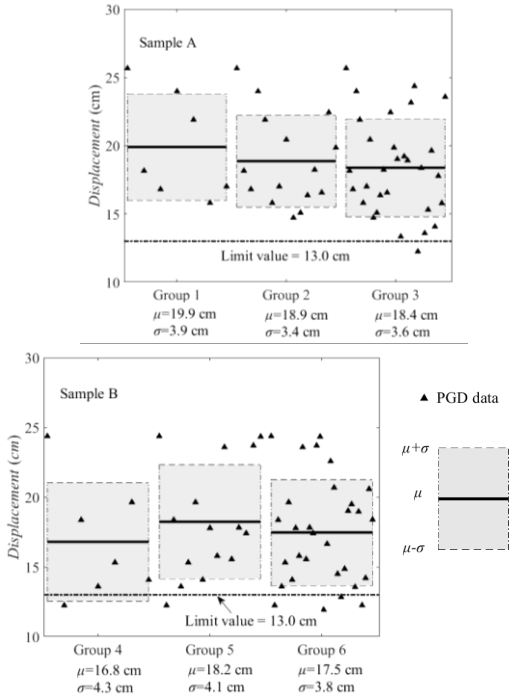

Fig. 8 Variation of PGDs with small sample-sizes

Table 2 Basic statistical values of PGDs with large sample-sizes

Group ID	*Number*	*μ (cm)*	*Min (cm)*	*σ (cm)*
7	*30*	*18.1*	*11.6*	*3.7*
8	*60*	*18.1*	*11.6*	*3.6*
9	*90*	*17.9*	*11.6*	*3.4*

practice, if a small number of simulated time-histories are selected as the seismic input, we do not know whether all the PGD results will satisfy the limit value. This motivates us to study how to control the PGD and its influence factors.

Next, we sampled all 90 time-histories into three groups with relatively larger sample sizes. The number of acceleration time-histories is 30, 60, and 90 for Group 7, Group 8, and Group 9, respectively, as shown in Table 2. The basic statistical values of PGD in these three groups are listed in Table 2, and their distributions are plotted in Fig. 9. It can be seen that the mean values of all PGD groups are higher than the limit value. However, PGD values lower than the limit value still exist, but the number of PGD values lower than the limit value cannot be determined.

More significantly, for groups with smaller sample sizes equaling to or less than 30 in Fig. 8 the means and standard errors of PGD samples vary more distinctively than these groups with larger sample sizes in Fig. 9. Therefore, a group with smaller sample-size may not represent the actual distribution of PGDs. Considering these results and the workload, we ultimately choose 30 as the reasonable sample size

4. Effects of ground motion simulation parameters on the distribution of PGD

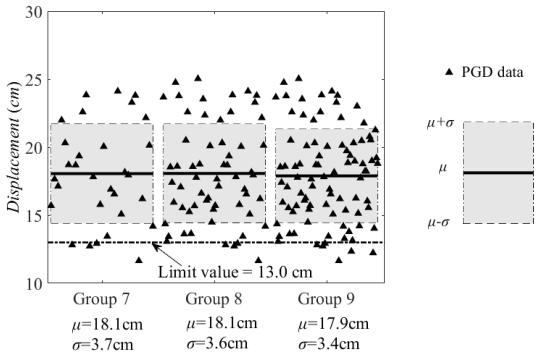

Fig. 9 Variation of PGDs with large sample-sizes

Based on the simulation method established in this paper, the artificial acceleration time-histories can be generated to match multiple targets, such as response spectra, PGAs, and nonstationarities in the intensity and frequency of ground motion. Therefore, the effects of the simulation parameters on the distribution of PGD can be discussed through fitting earthquake ground motion with different nonstationary characteristics.

4.1 Simulation scheme of ground motion

Two situations were set to complete this study, that is:

Situation I: nonstationarities in the intensity and frequency of ground motion are controlled during the simulation. Fitting conditions are listed as follows in detail.

1) The target spectrum is described by Eq. (19) with $A_{\max} = 200$ gal, $T_1 = 0.1$ s, $T_g = 0.4$ s, $T_m = 6$ s, and $\beta_m = 2.5$.

2) The intensity envelope function in the simulation is described as

$$E(t) = I_0(\mathrm{e}^{-\alpha_1 t} - \mathrm{e}^{-\alpha_2 t}) \tag{20}$$

Where I_0, α_1 and α_2 are modal parameters with $I_0 = 179.74$, $\alpha_1 = 0.1202$ and $\alpha_2 = 0.1230$.

3) $F_p(t)$, expressed by Eq. (8), was selected as the target of frequency change needed to approximately simulate the nonstationarity of ground motion frequency. We only selected 20 groups of parameters of $F_p(t)$ to simulate the acceleration time-histories. Their IDs, according to various magnitudes, epicenter distances and site conditions, are listed in Table 3, and the values of the parameters can be determined by the table found in Yu *et al.* (2015).

4) For each group, 30 initial ground motions were

Table 3 Group IDs according to magnitudes, epicenter distances and sites

M	(<5.5)		[5.5,6.5)		[6.5,7.5)		(≥ 7.5)	
R/km	20-40	40-60	20-40	40-60	20-40	40-60	20-40	40-60
Site A	1	Nan*	Nan*	2	3	4	5	6
Site B	7	Nan*	8	9	10	11	12	Nan*
Site C	13	14	15	16	17	18	19	20

*: no group

Table 4 Basic statistical values of PGDs for different groups in Situation I (S1) and Situation II (S2)

Group ID	S1 μ_1 (cm)	S2 μ_2 (cm)	Δμ (cm)	S1 Min_1 (cm)	S2 Min_2 (cm)	S1 σ_1 (cm)	S2 σ_2 (cm)	S1 CV_1	S2 CV_2	ΔCV
1	23.3	19.3	4.0	13.8	11.4	5.8	4.0	24.8	20.9	3.9
2	21.8	17.8	4.0	13.1	11.6	5.2	3.4	24.0	19.3	4.7
3	25.4	19.5	5.8	19.0	14.3	3.7	2.7	14.6	14.0	0.6
4	21.9	18.3	3.6	11.7	10.7	4.9	3.7	22.2	20.4	1.8
5	24.1	19.0	5.2	15.0	12.8	5.6	3.3	23.0	17.1	5.9
6	24.9	18.1	6.8	15.8	12.0	4.7	3.5	19.0	19.2	-0.2
7	21.2	18.5	2.7	11.1	11.2	5.4	4.0	25.3	21.8	3.4
8	21.5	18.1	3.4	14.3	10.4	3.6	4.2	16.9	23.3	-6.3
9	21.0	18.8	2.2	12.5	10.5	4.6	4.4	22.0	23.4	-1.4
10	22.5	19.4	3.1	12.4	11.8	5.6	4.1	24.9	21.3	3.6
11	20.5	18.6	1.9	10.9	11.4	6.2	5.0	30.4	26.9	3.6
12	20.8	19.2	1.6	10.3	13.1	4.4	3.8	21.0	19.5	1.4
13	21.6	18.7	2.9	16.3	10.5	3.2	4.4	14.6	23.7	-9.1
14	22.7	19.0	4.1	14.1	11.6	4.4	3.8	19.6	20.1	1.7
15	20.9	18.5	1.5	13.3	13.5	4.0	3.2	19.2	17.2	-0.1
16	22.7	19.0	2.8	14.1	11.6	4.4	3.8	19.6	20.1	-0.2
17	20.3	18.3	0.2	10.1	10.7	5.1	4.1	25.1	22.3	1.5
18	21.1	18.1	1.9	12.9	9.9	4.7	4.2	22.2	23.3	1.2
19	20.8	17.5	2.6	13.7	11.0	4.5	3.5	21.9	20.1	0.9
20	21.8	19.1	2.3	12.7	11.3	4.6	3.7	21.3	19.5	0.7

produced, using random phases. These time-histories were adjusted using Eqs. (13) and (18) to satisfy the given targets. Therefore, 600 time-histories can be obtained for 20 groups.

5) The limit values of PGD values are 11.7 cm for Site A, 13 cm for Site B and 18.2 cm for Site C, in accordance with Code GB50909-2014.

Situation II: only the nonstationarity of ground motion intensity was taken into account in the simulation.

1) The target spectrum, intensity envelope function and the limit value of the PGD were the same as those in Situation I.

2) The acceleration time-histories were generated according to the 20 groups in Situation I in which the initial random phase of each group is consistent with the corresponding group in Situation I. These time-histories were adjusted using Eqs. (17) and (18) to satisfy the given targets. Therefore, 600 time-histories without controlled F_p can be obtained for 20 groups.

In addition, the PGDs of the simulated time-histories were not controlled in either situation. The fitting errors between the target and modified spectra were constrained to be less than 5 percent. In every group, time-histories were not correlated with each other for the sake of the availability of the samples.

Finally, 1200 acceleration time-histories for 40 groups were generated to discuss the effect of controlling the ground motion non-stationary frequency on the distribution of PGD.

4.2 Comparison and analysis

First, we statistically analyzed PGDs in each simulated

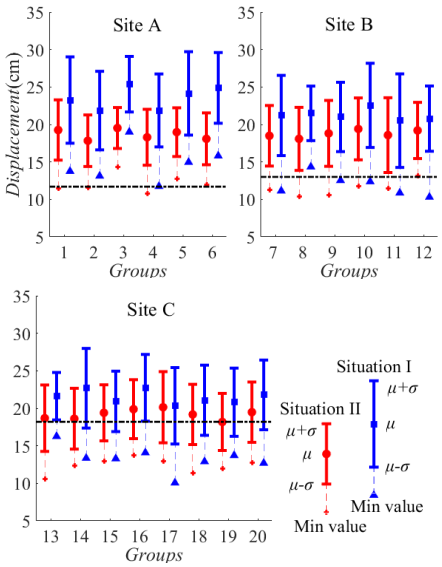

Fig. 10 Variations of the means, standard deviations and minimum values of PGDs

accelerograms group in the two different situations. The basic statistical values of all 40 groups are listed in Table 4 in which μ is the mean value, Min is the minimum value, σ is the standard deviation, and CV is the coefficient of variation of the normal distribution, representing the dispersion of samples with different means, that is

$$CV = \frac{\sigma}{\mu} \cdot 100\% \tag{21}$$

The greater the CV is, the more dispersed the samples. Then, for easy comparison, we define the difference in the respective CVs between Situation I and Situation II as ΔCV, that is

$$\Delta CV = CV_1 - CV_2 \tag{22}$$

in which CV_1 and CV_2 are the coefficients of variation controlling F_p (Situation I) and not controlling F_p (Situation II) respectively. ΔCV represents the change in the dispersion between the predominant frequency-controlling and not controlling situations. If $\Delta CV > 0$,the dispersion increases when we control F_p; otherwise, it decreases.

The variations of the PGD mean, standard deviation and minimum values for Situation I and Situation II are plotted in Fig. 10. It can be seen that compared with Situation II, the mean values of the PGD increase significantly and the number of PGDs lower than the limit value decreases when the predominant frequency is controlled (Situation I).

Particularly for Site A, all the PGD values are greater than the limit value when controlling the frequency nonstationarity (Situation I). For Site C, even the mean PGD values may be less than the limit value (Group 19), when only the ground motion intensity nonstationarity was taken into account in the simulation, which can be clearly improved in Situation I.

The ΔCV values of all 20 group pairs are plotted in Fig. 11(a). It can be seen that only 6 pairs of groups exhibit a ΔCV less than zero. This result indicates that the dispersion

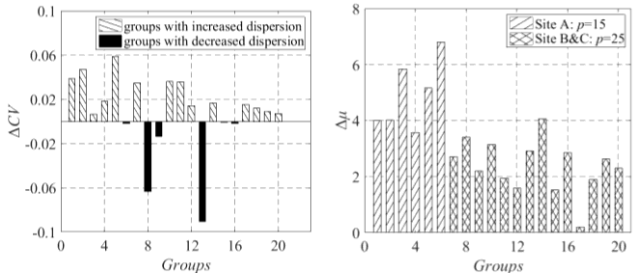

(a) Variation of ΔCV (b) Variation of $\Delta\mu$

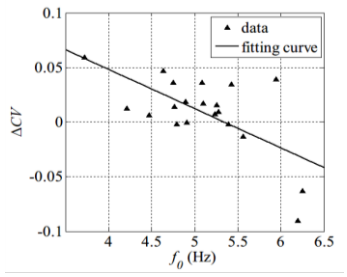

(c) Fitting results between ΔCV and f_0

Fig. 11 Variation of ΔCV and $\Delta\mu$ between Situation I and II

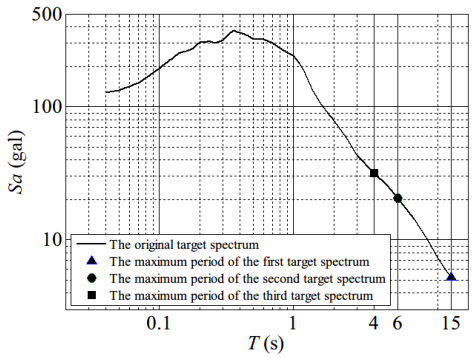

Fig. 12 Target response spectra and maximum values of period

Table 5 Basic statistical values of peak displacements (cm)

T_m	Mean	Min	σ	CV (%)
4 s	9.5	5.6	2.1	22.4
6 s	10.2	6.9	2.1	20.1
15 s	12.6	9.2	1.8	19.8

of the corresponding PDG distribution cannot be reduced by controlling the frequency variation when simulating ground motion. Therefore, we tried to find the reasons by analyzing the changes in the mean and dispersion of the PGD before and after controlling $F_p(t)$. The results show that the difference in the mean values between the two situations, $\Delta\mu = \mu_1 - \mu_2$, as listed in the 4th column in Table 4, is correlated to the modal parameter p in Eq. (8). The value of $\Delta\mu$ when $p = 15$ is greater than that when $p = 25$, as shown in Fig. 11(b). Moreover, the variation in ΔCV is significantly correlated with the parameter f_0, representing the approximate range of the initial predominant frequencies given in Eq. (8), as shown in Fig. 11(c). There is a negative linear relationship between these factors, that is, the dispersion increases when the initial predominant frequencies decrease.

In brief, the mean value of the ground motion PGD can be increased by controlling the frequency nonstationarity of the simulated ground motion, but their dispersion cannot be reduced effectively. Additionally, the effects of the simulated ground motion frequency variation on the PGD distributions correlate to its predominant frequency modal parameters.

5. Effects of the maximum period of the target spectrum on the distribution of PGDs

According to the definition of the ground motion acceleration response spectrum, the PGD can be estimated by the spectral values that correspond to longer periods. However, the maximum period (T_m) of response spectra applied in engineering designs is generally less than 6 s. For long-period structures, the design response spectra with longer periods can be obtained through seismic hazard analysis. Whether the maximum period of the target response spectra affects the simulated ground motion PGD distribution is a question that we need to discuss in this section.

In this study, a long-period acceleration response spectrum with $T_m = 15\text{s}$ is adopted. Three target spectra can be formed by cutting off the spectrum in different periods, that is, the period ranges of the target spectra are set to (0-4) s, (0-6) s and (0-15) s, as shown in Fig. 12. Then, 30 acceleration time-histories with random initial phases were adjusted with Eqs. (17) and (18) for every target, and 90 time-histories can be obtained for three target spectra. In the simulation, to ensure that the variation in PGD dispersion is only due to the change in T_m, the conditions are set as follows:

1) The PGAs were set to 128.6 gal for the three different spectra.
2) For the three different target spectra, the initial 30 random phases are the same when generating the initial ground motions.
3) Only the intensity nonstationarity of the ground motion was considered, and the intensity envelope function was the same for the three different spectra. Therefore, Eqs. (17) and (18) were used to adjust the initial ground motions to ensure that they were compatible with the target spectrum.
4) The PGD was not controlled during the simulation of ground motion.

In addition, baseline correction was carried out in the simulation, and the errors between the modified and target spectra were controlled to less than 5%.

Then, the distributions of the PGD for the three groups were discussed based on the 90 synthesized ground motions. The PGD limit value was 7 cm in this case, in accordance with Code (GB50909-2014).

The basic statistical values of the PGD for the three groups are listed in Table 5, and the PGD distributions for the three groups are plotted in Fig. 13. It can be seen that both the mean and minimum values of the PGD increase

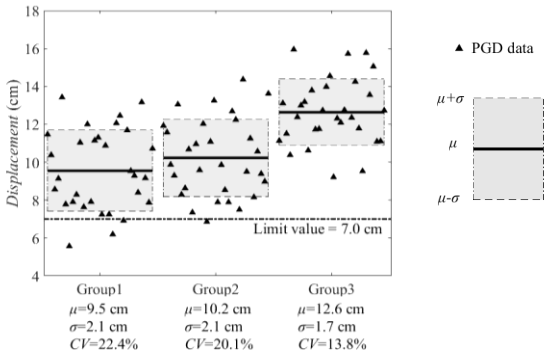

Fig. 13 Distribution plots of the means and standard deviations of PGDs for three different spectra

with increasing T_m. Moreover, when $T_m = 15$ s, the PGD tends to concentrate to the mean values, representing a lower dispersion. Even the minimum value, 9.21 cm, meets the requirement of the Code.

As discussed above, the dispersion can be decreased by extending the maximum period of the target spectrum. Meanwhile, the mean increases. Thus, if the maximum period T_m is greater than 15 s, the simulated ground motion PGD can be well controlled.

6. Simulation method for earthquake ground motions with required PGD values

6.1 Basic adjustment method

As discussed above, when fitting the acceleration time-history based on the target spectrum, the corresponding PGD may not satisfy the limit value in the Code if the PGD is not controlled. Although a much greater maximum period in the target spectrum can control the PGD more effectively, no current engineering codes provide design spectra with periods extending to 15 s. Therefore, for some long-period structures sensitive to the PGD of the seismic input, the control of the PGD in simulation is essential. Therefore, we revised the ground motion simulation method to satisfy multiple targets, including the required PGD limit value.

Adjusting the acceleration time-history $a_g^{i+1}(t)$ at ω_k using Eqs. (13)-(18) and integrating over time, the corresponding displacement time-history can be obtained. Defining the peak displacement as D_p, the difference ΔD between D_p and the target PGD (D_p^T) can be determined as

$$\Delta D = D_P - D_P^T \tag{23}$$

The incremental displacement time-history $\Delta d_g(t)$ at ω_k can be defined using a cosine functions, such as

$$\Delta d_g(t) = -\text{sgn}[\Delta D]\frac{\Delta D}{R}\text{e}^{\zeta\omega_k(t-t_{md})}\cos(\omega_{kD}t + \phi_{kd}), \quad t \le t_{md} \tag{24}$$

where t_{md} is the time corresponding to the peak displacement response of the single-degree system, ϕ_{kd} is the adjusting phase of the PGD, ζ is the damping ratio, ω is the circular frequency, and R is defined as an amplifying factor, which can be determined according to the demanded precision.

Calculating the second deviation of Eq. (24) with respect to t, we can determine the acceleration incremental time-history corresponding to $\Delta d_g(t)$, that is

$$\Delta\bar{a}_g(t) = -\text{sgn}[\Delta D]\cdot\frac{\Delta D}{R}\cdot\text{e}^{\zeta\omega_k(t-t_{md})} [\omega_k^2(\zeta^2-1)\cos(\omega_k t + \phi_{kd}) - 2\zeta\omega_k^2\sin(\omega_k t + \phi_{kd})], \quad t \le t_{md} \tag{25}$$

To maintain the characteristics of ground motion, $\Delta\bar{a}_g(t)$ at ω_k should be adjusted by taking into account the time modulating function $B(t, \omega_k)$ with

$$\Delta a_g(t) = \Delta\bar{a}_g(t)B(t, \omega_k) \tag{26}$$

Then, the acceleration time-history $a_g^{i+1}(t)$ with the adjusted PGD can be represented as

$$Da_g^{i+1}(t) = a_g^{i+1}(t) + \Delta a_g(t) \tag{27}$$

Applying the results, $Da_g^{i+1}(t)$ of every adjustment step as the initial input at the next controlling period, an iterative procedure can be carried out to relieve the

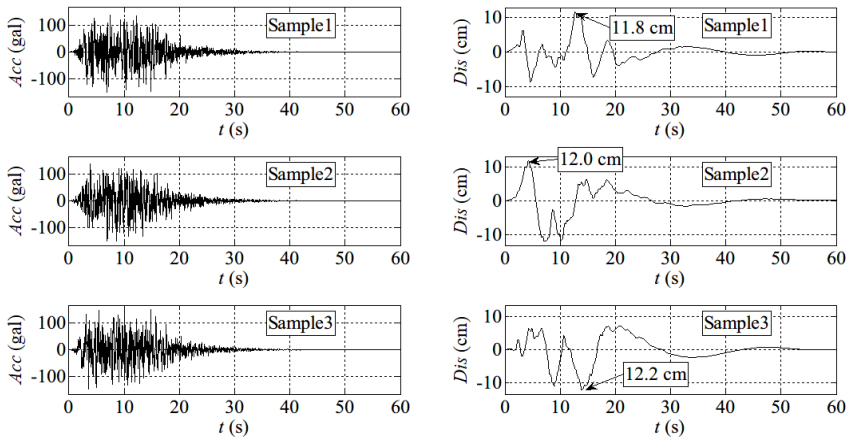

Fig. 14 Artificial acceleration time-histories compatible with target response spectrum and corresponding displacement time-histories

influence of the adjustment on the response for previous controlling periods. Finally, we can obtain artificial ground motion that is compatible with the target spectrum and meets the required PGA and the limit PGD values.

6.2 Example

An example is used to illustrate the control of the PGD in the simulation. The target response spectrum is described by Eq. (19) in which the PGA=150 gal, $\beta_m = 2.7$, $\gamma = 1.0$, $T_g = 0.5$ s , $T_m = 6$ s. According to the PGA and the site condition, the limit value of the PGD listed in Code (GB50909-2014) is 10.2 cm. In this section, we used the method proposed in Section 5.1 to generate ground motion compatible with multiple targets, in particular, with the target PGD values. In the simulation, the amplitude envelope is selected as shown in Fig. 7, with $t_1 = 3.5$ s, $t_2 = 15.5$ s, and $t_d = 60$s. A total of 74 periods between 0.04 s and 6 s are selected to control the form of the target spectrum and are evenly distributed in the logarithmic coordinate. To reflect the diversity of the samples, three different peaks of displacements, 11.8 cm, 12.0 cm and 12.2 cm, are set as PGD targets to generate spectrum-compatible acceleration time-histories. Using the revised method developed in Section 5.1, we successfully simulate three acceleration time-histories, as shown in Fig. 14. The relative maximum errors between the modified and target spectra of samples 1, 2, and 3 are 2.4%, 2%, and 3%, respectively, and the PGD is controlled to meet the targets without error. Therefore, the method proposed in this study is a good option for simulating ground motion for seismic designs.

7. Conclusions

In this study, we develop a simulation method for ground motion matching of multiple targets. Based on this method, artificial ground motion, based on different controlling parameters, is generated to analyze the distribution of the corresponding PGD. The conclusions obtained in this study are as follows:

1) The ground motion simulation method developed in this study can not only match multiple targets, such as the PGA and the spectrum, but can also simulate the nonstationarity of earthquake ground motion frequency by introducing a frequency-dependent amplitude envelope function with statistical parameters.

2) In the simulation of spectrum-compatible artificial ground motions, if the acceleration time-histories are generated with random initial phases and the corresponding PGD is not controlled, the PGD distribution is quite discrete. Additionally, PGD values lower than the limit value are observed, but the number of PGD values lower than the limit value is uncertain. However, the PGD mean values always meet the requirement in each group, and the degree of dispersion is independent of the number of accelerograms in each group.

3) If the nonstationary frequency of the ground motion is taken into account when simulating the acceleration time-histories, the PGD mean values will increase, but the dispersion will not decrease effectively. Correlation analysis shows that the change in the mean and dispersion, from before the frequency is controlled to after, correlates to the predominant frequency modal parameters.

4) Extending the maximum period of the target spectrum will increase the corresponding PGD value. Simultaneously, the PGD dispersion will decrease. In particular, when the maximum controlling period is greater than 15 s, the PGD will have a relatively concentrated distribution.

5) Finally, the ground motion simulation method suggested in this study is revised by adding a specified PGD as one of the targets. This novel method can generate ground motion satisfying not only the required precision of the target spectrum, PGA, and nonstationarity characteristics of the ground motion but also the PGD requirement. The engineering example shows that this method has good precision and is convenient for engineering applications.

Acknowledgement

The financial supports from National Key R & D Program of China (2017YFC0404901) and Natural Science Foundation of China (No. 51878627 and No. 51478440) are much appreciated.

Reference

Amin, M. and Ang A.H.S (1968), "Nonstationary stochastic models of earthquake motions", *J. Eng. Mech.*, ASCE, **94**(2), 559-584.

Boashash, B. (1992a), "Estimating and interpreting the instantaneous frequency of a signal-part 1: Fundamentals", *Proc. IEEE*, **80**(4), 520-538. https://doi.org/10.1109/5.135376.

Boashash, B. (1992b), "Estimating and interpreting the instantaneous frequency of a signal-part 2: Algorithms and applications", *Proc. IEEE*, **80**(4), 540-568.

Boore, M.D. (2005), "On pads and filters: processing strong-motion data", *Bull. Seismol. Soc. Am.*, **95**(2), 745-750. https://doi.org/10.1785/0120040160.

Buratti, N. and Tavano, M. (2014), "Dynamic buckling and seismic fragility of anchored steel tanks by the added mass method", *Earthq. Eng Struct. Dyn.*, **43**, 1-21. https://doi.org/10.1002/eqe.2326.

Cacciola, P. (2010), "A stochastic approach for generating spectrum compatible fully nonstationary earthquakes", *Comput. Struct.*, **88**(15-16), 889-901. https://doi.org/10.1016/j.compstruc.2010.04.009.

Carballo, J.E. and Cornell, C.A. (2000), "Probabilistic seismic demand analysis: Spectrum matching and design", Report No. RMS-41, Department of Civil and Environmental Engineering, Stanford University.

Castagna, J.P., Sun, S.J. and Siegfried R.W. (2003), "Instantaneous spectral analysis: detection of low-frequency shadows associated with hydrocarbons", *Lead. Edge*, **22**(2), 120-127. https://doi.org/10.1190/1.1559038.

Clough R.W. and Penzien J. (1975), *Dynamics of Structures*,

McGraw-Hill, New York U.S.A.

Converse, M.A. and Brady, G.A. (1992), "BAP: Basic Strong-Motion Accelerogram Processing Software: Version 1.0," Open-File Report 92-296A, United States Department of The Interior U.S. Geological Survey.

Gao, Y.F., Wu, Y.X., Li, D.Y., Zhang, N. and Zhang, F. (2014), "An improved method for the generating of spectrum-compatible time series using wavelets", *Earthq. Spectra*, **30**(4), 1467-1485. https://doi.org/10.1193/051912EQS190M.

GB50909-2014 (2014), Code for Seismic Design of Urban Rail Transit, Ministry of Construction of People's Republic of China, Beijing, China. (in Chinese)

Ghaboussi, J. and Lin, C.J. (1998), "New method of generating spectrum compatible accelerograms using neural networks", *Earthq. Eng. Struct. Dyn.*, **27**, 377-396. https://doi.org/10.1002/(SICI)1096-9845(199804)27:4<377.

Guan, M.S., Du, H.B., Cui, J., Zeng, Q.L. and Jiang, H.B. (2015), "Optimal ground motion intensity measure for long-period structures", *Measure. Sci. Technol.*, **26**(10), 105001.

Hall, J.F., Heaton, T.H., Halling, M.W. and Wald, D.J. (1995), "Near-source ground motion and its effects on flexible buildings", *Earthq. Spectra*, **11**(4), 569-605. https://doi.org/10.1193/1.1585828.

Han, M., Duan, Y.L., Sun, H. and Sheng, W. (2013), "Influence of characteristics parameters of near-fault ground motions on the seismic responses of base-isolated structures", *China Civil Eng. J.*, **46**(6), 8-13. (in Chinese)

Hancock, J., Watson-Lamprey, J., Abrahamson, N.A., Bommer, J.J., Markatis, A., McCOTH, E. and Mendis, R. (2006), "An improved method of matching response spectra of recorded earthquake ground motion using wavelets", *J. Earthq. Eng.*, **10**(S1), 67-89.

Huang, N.E., Shen, Z., Long, S.R., Wu, M.C., Shin, H.H., Zheng, Q., Yen, N.C., Tung, C.C. and Liu, H.H. (1998), "The empirical mode decomposition and the Hilbert spectrum for nonlinear and non-stationary time series analysis", *Proc. R. Soc. Lond. A*, **454**(1971), 903-995. https://doi.org/10.1098/rspa.1998.0193.

Iwan, W.D., Moser, M.A. and Peng, C.Y. (1985), "Some observations on strong-motion earthquake measurement using a digital accelerograph", *Bull. Seismol. Soc. Am.*, **75**(5), 1225-1246.

Iyengar, R.N. and Iyengar, K.T.S.R. (1969), "A nonstationary random process model for earthquake accelerograms", *Bull. Seismol. Soc. Am.*, **59**(3), 1163-1188.

Lilhanand K. and Tseng W.S. (1988), "Development and application of realistic earthquake time histories compatible with multiple-damping design spectra", *Proceedings of Ninth World Conference on Earthquake Engineering*, Tokyo, August.

Milana, G., Rovelli, A., Sortis, A.D., Calderoni, G., Coco, G., Corrao, M. and Marsan, P. (2008), "The role of long-period ground motions on magnitude and damage of volcanic earthquakes on Mt. Etna, Italy", *Bull. Seismol. Soc. Am.*, **98**(6), 2724-2738. https://doi.org/10.1785/0120080072.

Mukherjee, S. and Gupta, V.K. (2002) "Wavelet-based generation of spectrum-compatible time-histories", *Soil Dyn. Earthq. Eng.*, **22**, 799-804. https://doi.org/10.1016/S0267-7261(02)00101-X.

Naeim, F. and Lew, M. (1995), "On the use of design spectrum compatible time histories", *Earthq. Spectra*, **11**(1), 111-127. https://doi.org/10.1193/1.1585805.

Newland, D.E. (1994), "Wavelet analysis of vibration: Part 2-wavelet maps", *J. Vib. Acoust.*, **116**(4), 417-425. https://doi.org/10.1115/1.2930444.

Nigam, N.C. and Mark, W.D. (1984). "Introduction to random vibrations", *J. Acoust. Soc. Am.*, **76**(6), 1871. https://doi.org/10.1121/1.391500.

Pineda-Porras, O. and Ordaz, M. (2007), "A new seismic intensity parameter to estimate damage in buried pipelines due to seismic wave propagation", *J. Earthq. Eng.*, **11**(5), 773-786. https://doi.org/10.1080/13632460701242781.

Preumont, A. (1984), "The generation of spectrum compatible accelerograms for the design of nuclear power plants", *Earthq. Eng. Struct. Dyn.*, **12**(4), 481-497. https://doi.org/10.1002/eqe.4290120405.

Rezaeian, S. and Kiureghian, A.D. (2008). "A stochastic ground motion model with separable temporal and spectral nonstationarities", *Earthq. Eng Struct. Dyn.*, **37**, 1565-1584. https://doi.org/10.1002/eqe.831.

Rezaeian, S. and Kiureghian, A.D. (2010), "Simulation of synthetic ground motions for specified earthquake and site characteristics", *Earthq. Eng Struct. Dyn.*, **39**, 1155-1180. https://doi.org/10.1002/eqe.997.

Tondini, N. and Stojadinovic, B. (2012), "Probabilistic seismic demand model for curved reinforced concrete bridges", *Bull. Earthq. Eng.*, **10**, 1455-1479. https://doi.org/10.1007/s10518-012-9362-y.

Yu, R.F., Yuan, M.Q. and Yu, Y.X., (2015), "Developed empirical model for simulation of time-varying frequency in earthquake ground motion", *Earthq. Struct.*, **8**(6), 1463-1480. http://dx.doi.org/10.12989/eas.2015.8.6.1463.

Zhao, F.X., Zhang, Y.S. and Lü, H.S. (2006), "Artificial ground motion compatible with specified ground shaking peaks and target response spectrum", *Earthq. Eng. Eng. Vib.*, **5**, 41-48. https://doi.org/10.1007/s11803-006-0625-y.

CC